Truncated-correlation photothermal coherence tomography derivative imaging modality for small animal *in vivo* early tumor detection

HAI ZHANG,[1,3,†] 🄳 PANTEA TAVAKOLIAN,[1,†] 🄳 KONESWARAN SIVAGURUNATHAN,[1] ANDREAS MANDELIS,[1,*] WEI SHI,[2] AND FEI-FEI LIU[2]

[1]*Center for Advanced Diffusion-Wave and Photoacoustic Technologies (CADIPT), Department of Mechanical and Industrial Engineering, University of Toronto, Toronto, Ontario M5S 3G8, Canada*
[2]*Princess Margaret Cancer Center, University Health Network, Toronto, Ontario M5G 2M9, Canada*
[3]*e-mail: hzhang@mie.utoronto.ca*
Corresponding author: mandelis@mie.utoronto.ca

Early cancer non-invasive diagnosis is a leading medical topic worldwide due to the threat to human life and the high death rate of this disease. Light-absorption-based thermophotonic diagnostic imaging is well positioned for this challenge thanks to its speed, safety, and high molecular contrast advantages. In this Letter, an enhanced truncated-correlation photothermal coherence tomography (TC-PCT) imaging modality is presented for early *in vivo* tumor detection and tested using a nude mouse thigh. Compared with conventional TC-PCT, the enhanced imaging modality was found to exhibit higher contrast that contributed to the precise measurement of the size and shape of the detected tumor. The experimental results were validated following histological analysis from hematoxylin and eosin staining. This increased contrast advantage gives rise to possible clinical applications in early tumor detection and treatment and in monitoring the effects of anti-tumor drugs. © 2019 Optical Society of America

Cancer is one of the leading causes of death worldwide. In 2018, an estimated 1,735,350 new cases of cancer will be diagnosed in the United States, which will result in the death of 609,640 people from the disease. The number of new cases is estimated to rise to 23.6 million every year by 2030. In the United States, however, the cancer death rate has decreased since the early 1990s. These data show that effective efforts are being made against death caused by cancer, but more work remains to be done to enhance effectiveness, e.g., in early cancer detection and development of anti-tumor drugs [1].

Several tumor hypoxia assessment modalities have been proposed, but none have been used in clinical practice. Among them, polarographic electrodes are the current benchmark for tumor hypoxia detection. However, they are highly invasive and require highly technical skills. Therefore, measurement repeatability is extremely challenging. Moreover, hypoxia over-estimation often occurs in necrotic sample regions using this method, since the probe is unable to identify differences between living and necrotic tissues [2].

Medical ultrasound (US) is useful for diagnostic assessment of palpable mass analysis, identifying solid masses or cysts or guiding biopsies. However, US, too, is unable to diagnose early cancer since it cannot reveal anatomical and morphological differences between the tumor and healthy tissues.

Alternatively, biomedical photothermics (PT) is a non-ionizing, non-invasive diagnostic methodology. It is based on spectrally selective optical absorption of modulated (or pulsed) electromagnetic radiation, thermal (non-radiative) conversion, and generation of thermal waves in tissues. Thermophotonic imaging (TPI) is an emerging PT diagnostic modality [3] currently being explored for early cancer diagnosis. It involves the detection of photothermal waves through emitted infrared (IR) photons (Planck radiation) from tissue using mid-IR cameras. TPI, like its photoacoustic (PA) counterpart, combines high optical contrast and spectroscopic specificity with high spatial resolution [4]. However, unlike PA imaging, TPI has the advantage of remote, air-coupled inspection without the need for, and complications of, a coupling fluid to transmit the signal to the transducer.

The field of biomedical TPI techniques has undergone significant growth in the past decade, including instrumentation development, image reconstruction algorithms, and *in vitro* applications in basic biological research [5]. Among all potential practices, early cancer detection and monitoring the effects of anti-tumor drugs in real time are extremely attractive due to their huge health care implications and market value: estimated national expenditures for cancer care in the United States in 2017 were $147.3 billion. In the next few years, costs are expected to rise as the population ages and cancer prevalence increases. Costs are also expected to rise as new, and often more expensive, treatments are adopted as standards of care [1].

The growth of tumor cells (hypermetabolism) raises nutrients and oxygen consumption compared to healthy tissue, and therefore, it results in the development of dense vascular networks (i.e., angiogenesis). This is a critical indicator of the

onset of cancerous lesion growth. The sensitivity of TPI to oxygenated hemoglobin concentration can potentially quantify these hallmarks of cancer and facilitate its early detection via enhanced laser light absorption in the 650–1100 nm tissue optical window spectral range [2].

In this Letter, a thermophotonic (TP) image generation modality is presented, aimed at making early developing tumors such as one injected in a live mouse thigh, optimally detectable. The new imaging modality is based on truncated-correlation photothermal coherence tomography (TC-PCT) [6,7]. The goal of the ensuing imaging is to provide higher contrast than conventional TC-PCT images and make a precise measurement of tumor size and shape. The experimental results bore out the success of the new modality: the size and shape of an early tumor were detected for the first time, to the best of our knowledge, using TPI, and its surrounding dense vascular network became more clearly identifiable early in its growth phase with high contrast. This improvement is highly desirable for clinical diagnosis. The non-invasive TC-PCT diagnostic results were also validated by a histopathological study. To the best of our knowledge, this is the first time that an *in vivo* early tumor and its surrounding dense vascular network were detected with high contrast, spatial and axial resolution using non-invasive TPI exhibiting significantly higher specificity than US imaging [2,4].

In the conventional TC-PCT technique [6], the truncation slice range depends on the laser excitation pulse width W. Accordingly, the TC-PCT slice width changes from $t = 0$ to $t = W$. In a later version of the TC-PCT technique [7], there was no relation between the excitation pulse width W and the TC-PCT slice width as a result of filtering. W was selected based on a desirable total energy delivered to the tissue, while the TC-PCT slice width was selected to obtain high SNR images with moderate axial resolution. Therefore, the laser energy was less than the maximum permissible exposure (0.79 J/cm^2 for chirp duration of 83 s) [8]. This is an important feature toward clinical applications of the TC-PCT technique.

In the present new TC-PCT imaging modality, the conventional TC-PCT images were processed using the procedure shown in Fig. 1. Following median and Gaussian filters, polynomial regression and derivative processing were applied. In polynomial regression, the logarithmic time dependence of a pixel can be approximated by a function or a set of orthogonal functions as follows [9]:

$$\ln[A(t)] = \sum_{0}^{N} a_n [\ln(t)]^n, \tag{1}$$

where A values are registered along the y axis, and t denotes the time (slices) displayed along the x axis.

Then, a fourth-order expansion was used as a low-pass filter. This is because in the logarithmic domain, high orders only replicate noise (which appears in the low-amplitude data). According to Eq. (1), once the time evolution of each pixel has been approximated, the original data can be reconstructed on a logarithmic scale as follows [9]:

$$A(t) = \exp\left(\sum_{0}^{N} a_n [\ln(t)]^n \right). \tag{2}$$

According to Eqs. (1) and (2), it is possible to only save the polynomial coefficients regardless of the length of the image sequence. More details regarding polynomial regression can be found elsewhere [9].

It has been found that derivative processing can provide clearer internal detection information thanks to contrast enhancement by virtue of taking the slope of a function or distribution [9]. Subsequently, the above-processed new image sequences, including the logarithmic reconstruction time-evolution sequences and their saved derivative-processed results, were post-processed through the use of principal component thermography and empirical orthogonal functions (EOFs) [10]. This method can provide a group of orthogonal statistical modes derived from geophysics [11]. The orthogonal statistical models can give the strongest projection for the image sequences, and also provide a few compact variations. EOFs are calculated on the basis of singular value decomposition (SVD) of the image sequences. In detail, $N \times M$ matrix A was first decomposed as follows [10]:

$$A = U\tau V^T, \tag{3}$$

where $-\tau$ is an $N \times N$ diagonal matrix with positive or zero elements that represent the singular values of matrix A, U is an $M \times N$ matrix, and V^T is the transpose of an $N \times N$ matrix.

If matrix A is arranged so that the time variations are column-wise and spatial variations are row-wise, the columns of the matrix U consist of a group of EOFs that can represent the spatial variations in the time evolution. SVD extracts a group of compact spatial, temporal, and time variations from matrix A by projecting the original image sequences onto the EOFs. Then, the original image sequences can be represented by only a few images (EOFs). This method features an excellent noise-rejection capability, and more discussion about it can be found elsewhere [10].

The complete schematic diagram of the new imaging modality is shown in Fig. 1. IR_VIEW software (Visiooimage, Canada) was used as an assistance tool in MATLAB environment.
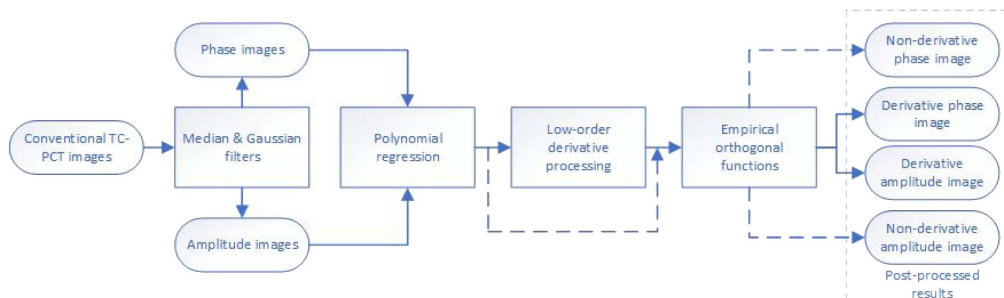

Fig. 1.   Schematic diagram of the TC-PCT enhanced imaging modality.

Human hypopharyngeal head and neck squamous cell carcinoma FaDu cell lines were obtained from the American Type Culture Collection (Manassas, VA) and cultured in minimal essential medium (MEM) F-15 supplemented with 10% fetal bovine serum. The left thigh of a nude mouse was injected subcutaneously with 4.8×10^6 cultured cells/30 μL and imaged consecutively over a three-week period (results are presented for one session). The animal was fully anesthetized throughout the experiment by administering 1 L/min of oxygen mixed with isoflurane gas (3% for induction and 1–1.5% for maintenance). An IR heating lamp was used to regulate the animal body temperature. The experiments were approved by the Division of Comparative Medicine (DCM), the Faculty of Medicine, University of Toronto, under the guidelines of animal protocol 20011804.

Figure 2 shows the experimental setup and a photograph of the imaged live nude mouse with the tumor in its left thigh. In the experimental setup, the excitation source was an 808 nm diode laser (Jenoptic JOLD-120-QPXF-2P) connected to a laser driver (PCO-6131, Directed Energy, Colorado, USA). The system was controlled by a waveform generator (Keysight 33500B, USA). The laser output was coupled to an optical fiber and passed through a collimator (F22SMA-B, Thorlabs Inc., New Jersey, USA). A diffuser (ED1-C20, Thorlabs Inc., New Jersey, USA) produced beam intensity homogenization before irradiating the mouse. A 3–5 μm spectral band IR camera (A6700sc, FLIR, USA) was used to capture the emitted thermal radiation. A computer controlled the entire system by executing the experimental TC-PCT algorithm in LabView software. The camera recorded a video in the FLIR format (Research IR Max 4, V.4.20.2, USA). Each frame of the video was exported as a text file containing the data for each image pixel. Then, they were imported in the LabView environment. Subsequently, the camera frames were synchronized with the corresponding excitation signal recorded by a high-speed data acquisition module (NI PCI-6281), and a post-processing algorithm reconstructed images from the IR frames recorded by the camera. Imaging parameters were in the frequency range between 0.07 and 0.1 Hz, pulse duration 83 s, excitation pulsewidth (W) 70 ms, and reference sliced width (ΔW) 100 ms. The frame size was 13.5 mm × 10.8 mm, and the lateral resolution was 42 μm.

Figure 3 shows the conventional TC-PCT pre-injection left thigh images. These dynamic TP images exhibit contrast depending on the absorption coefficient at the excitation wavelength. As shown in Fig. 3, blood vessels provide higher thermal-wave amplitudes than surrounding tissues due to the increased absorption coefficient of hemoglobin compared to surrounding tissues. In the pre-injection images, no tumor-like objects were visible, as expected.
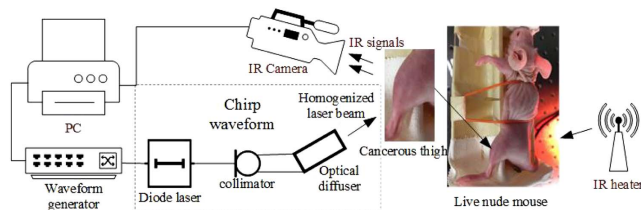

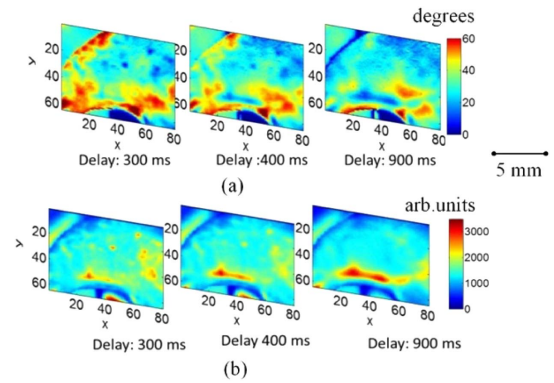**Fig. 2.** Experimental configuration and photograph of the cancer-cell-injected thigh.

Fig. 3. Conventional TC-PCT images without a tumor: (a) phase images and (b) amplitude images.

Figure 4 shows the conventional TC-PCT images on the nineth day after injection, which exhibits an early diagnostic result for the tumor. The images show an identifiable tumor from this injection day. The tumor was invisible with the naked eye and could not be detected with high spatial resolution using other non-invasive techniques (PA imaging and US) [2,4]. In Fig. 4, the vasculature network around the tumor is clearly visible. Accordingly, the presence of a tumor in the core of the vasculature network could be expected [12]. However, the core (tumor) is not as clearly visible as its surrounding vasculature network, and thus the tumor size and shape cannot be clearly identified and measured from the images. In conclusion, the conventional TC-PCT images can herald the presence of the tumor at an early stage; however, images of a more clearly identifiable tumor, including its size and shape, are highly desirable toward clinical diagnosis applications.

Figure 5 exhibits the improvement and advantages of the new imaging modality. The color bar units in Fig. 5 reflect the changes of the gradient vectors, which are based on the phase or amplitude slices in the conventional TC-PCT results. As discussed previously, the conventional TC-PCT phase and amplitude images after 300 ms clearly show the vasculature surrounding the core (tumor), but the color of the tumor is similar to that of the surroundings, making it hard to identify it. The 400 ms image is optimal, clearly showing the best contrast. In Figs. 5(a) and 5(c), the vasculature in the non-derivative-processed images is clearly visible as in Fig. 4, and
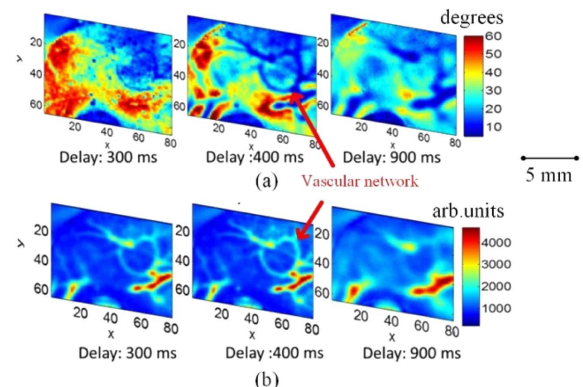

Fig. 4. Conventional TC-PCT images with an early period tumor: (a) phase images and (b) amplitude images.
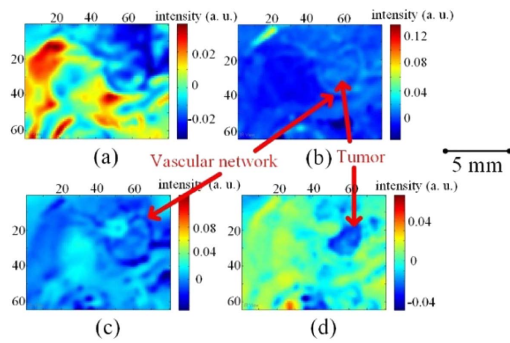
Fig. 5. Results of the new image generation modality (linked to Fig. 4): (a) non-derivative phase image, (b) derivative phase image, (c) non-derivative amplitude image, and (d) derivative amplitude image.

Fig. 6. Histopathological validation. The two green quadrangles in the middle of the tumor indicate the in-software measured sizes, which are identified in the photo.

there is additional color gradation inside the tumor compared to its surroundings. In the derivative-processed *amplitude image*, the tumor is very clear, but the surrounding vasculature has faded, as shown in Fig. 5(d). In the derivative-processed *phase image*, Fig. 5(b), the tumor and its surrounding vasculature are both identifiable, but the tumor is not as clearly visible as in the derivative amplitude image. The combination of both derivative-processed images, amplitude and phase, can clearly identify the tumor and the surrounding vasculature. This type of information cannot be obtained from the conventional TC-PCT images. In summary, the derivative-processed amplitude exhibits the highest tumor contrast, while the combined amplitude and phase images exhibit optimal tumor and surrounding vasculature specificity. This is because derivative processing provides the changes in the gradient vectors from all imaging slices, a process which enhances the changes of the micro and macro depth resolution while suppressing constant-level backgrounds.

The size of the tumor was measured to be 3 mm in the new image generation results in Fig. 5, a figure which was also independently verified. It was 0.5 mm thick and located 2 mm beneath the skin. In order to validate the TP measurement results, a histopathological study was conducted to confirm the presence of the cancerous tumor in the left thigh of the nude mouse. Hematoxylin and eosin (H&E) staining and immunohistochemistry (IHC) staining were performed on the excised tissue, and the stained sections were reviewed under a microscope.

H&E staining showed a cellular neoplasm arranged in nests and sheets (Fig. 6). The surrounding healthy tissue showed eosinophilic hyaline staining. It was concluded that the shape and size of the tumor in the new imaging modality results in Fig. 5 coincided with the histopathological profile. The excised tumor sample exhibited excellent correspondence with the image after euthanasia.

The present work demonstrates the introduction and successful application of the described new TC-PCT imaging modality for early cancer detection. To the best of our knowledge, it represents the first early tumor TP detection in a living animal. The new image generation methodology was shown to provide images with higher contrast and specificity in combined tumor and surrounding vasculature images than conventional TC-PCT, and it was able to yield precise measurements of the size and sha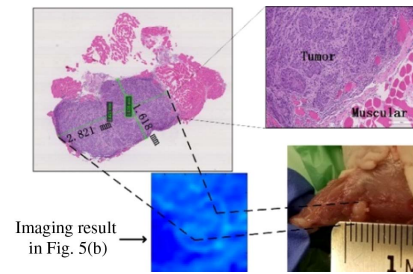pe of the tumor. The measurement results were validated using a histological study. In perspective, the present derivative tumor imaging method as applied to TC-PCT images heralds the possibility of using this photothermal modality to detect early cancers and/or monitor the effects of anti-tumor drug developments.

[†]These authors contributed equally to this work and should be considered co-first authors.

REFERENCES

1. "Cancer Statistics," Technical Report (National Cancer Institute [US], April 2018).
2. E. Dovlo, B. Lashkari, S. S. S. Choi, A. Mandelis, W. Shi, and F. F. Liu, J. Biophoton. **10**, 1134 (2017).
3. N. Tabatabaei, A. Mandelis, and B. T. Amaechi, J. Biomed. Opt. **16**, 071402 (2011).
4. E. Dovlo, B. Lashkari, A. Mandelis, W. Shi, and F. F. Liu, Biomed. Opt. Express **6**, 1003 (2015).
5. N. Tabatabaei, A. Mandelis, M. Dehghany, K. H. Michaelian, and B. T. Amaechi, J. Biomed. Opt. **17**, 025002 (2012).
6. S. Kaiplavil and A. Mandelis, Nat. Photonics **8**, 635 (2014).
7. P. Tavakolian, K. Sivagurunathan, and A. Mandelis, J. Appl. Phys. **122**, 023103 (2017).
8. "American National Standard for Safe use of Lasers," ANSI Z136.1–2007 (Laser Institute of America, 2007).
9. S. M. Shepard, J. R. Lhota, B. A. Rubadeux, D. Wang, and T. Ahmed, Opt. Eng. **42**, 1337 (2003).
10. N. Rajic, Compos. Struct. **58**, 521 (2002).
11. R. E. Thomson and W. J. Emery, *Data Analysis Methods in Physical Oceanography* (Elsevier, 2014), pp. 335–355.
12. R. K. Jain, Science **307**, 58 (2005).